Approaching ultrastrong coupling in transmon circuit QED using a high-impedance resonator

Sal J. Bosman,[1] Mario F. Gely,[1] Vibhor Singh,[2] Daniel Bothner,[1] Andres Castellanos-Gomez,[3] and Gary A. Steele[1]
[1]*Kavli Institute of NanoScience, Delft University of Technology, PO Box 5046, 2600 GA, Delft, The Netherlands*
[2]*Department of Physics, Indian Institute of Science, Bangalore 560012, India*
[3]*Instituto de Ciencia de Materiales de Madrid, CSIC, Madrid 28049, Spain*
(Received 24 April 2017; published 29 June 2017; corrected 18 December 2018)

In this experiment, we couple a superconducting transmon qubit to a high-impedance 645 Ω microwave resonator. Doing so leads to a large qubit-resonator coupling rate g, measured through a large vacuum Rabi splitting of $2g \simeq 910$ MHz. The coupling is a significant fraction of the qubit and resonator oscillation frequencies ω, placing our system close to the ultrastrong coupling regime ($\bar{g} = g/\omega = 0.071$ on resonance). Combining this setup with a vacuum-gap transmon architecture shows the potential of reaching deep into the ultrastrong coupling $\bar{g} \sim 0.45$ with transmon qubits.

DOI: 10.1103/PhysRevB.95.224515

I. INTRODUCTION

Cavity QED is a study of the light-matter interaction between atoms and the confined electromagnetic field of a cavity [1]. For an atom in resonance with the cavity, a single excitation coherently oscillates with vacuum Rabi frequency g between the photonic and atomic degree of freedom if g exceeds the rate at which excitations decay into the environment, which is known as the strong coupling condition [2]. Spectroscopically, this is observed as a mode-splitting (vacuum Rabi splitting) with distance $2g$. If the coupling is small with respect to the resonator (atomic) frequency ω_r (ω_a), $g \ll \omega_r, \omega_a$, and the frequencies respect the condition $|\omega_a - \omega_r| \ll |\omega_r + \omega_a|$, the interaction is faithfully described with the Jaynes-Cummings (JC) model [3]. As the coupling becomes a considerable fraction of ω_r or ω_a, typically $\bar{g} = g/\omega_{r,a} \sim 0.1$, the JC model no longer applies and the interaction is better described by the Rabi model [4–7]. This ultrastrong coupling (USC) regime shows the breakdown of excitation number conservation; however, excitation parity remains conserved for arbitrarily large $\bar{g}$ [8]. The key prediction for the deep-strong coupling (DSC) regime, where $\bar{g} \sim 1$, is a symmetry breaking of the vacuum (i.e., qualitative change of the ground state) similar to the Higgs mechanism [9]. The prospect of probing these new facets of light-matter interaction, in addition to potential applications in quantum information technologies [10,11], has spurred many experimental efforts to reach increasingly large coupling rates.

Experimentally, the only platform that observed ultrastrong or higher coupling rates with a single emitter uses a superconducting circuit with a flux qubit. Pioneered by the experiments of Refs. [12,13], experiments in the DSC regime have now been achieved with flux qubits coupled to resonators [14] as well as an electromagnetic continuum [15]. Additionally, the U/DSC coupling regime of the Rabi model was the subject of recent analog quantum simulations [16,17].

Here we explore coupling strengths at the edge of the USC regime in circuit QED using a superconducting transmon qubit [18] coupled to a microwave cavity that has a high characteristic impedance. Using a high-impedance Z_0 considerably increases coupling rates compared to typical 50 Ω implementations by increasing the voltage zero-point fluctuations of the cavity $V_{\mathrm{zpf}} \propto \sqrt{Z_0}$ as exploited in cavity QED with quantum dots [19]. When the transmon and fundamental mode of the cavity are resonant, we spectroscopically measure a coupling $g/2\pi = 455$ MHz, corresponding to $\bar{g} = 0.071$. With the prospect of maximizing the transmon analog of the dipole moment [20], we show how this system could approach its theoretical upper limit [21,22]

$$2g \lesssim \sqrt{\omega_r \omega_a}. \tag{1}$$

Exploring the ultrastrong coupling regime of the transmon has two main advantages with respect to using flux qubits. First, the transmon has become a standard in efforts to build a quantum processor [23–25]. Implementing USC in this system therefore paves the way to exploiting USC features in quantum computation to decrease gate times [10] and perform quantum error correction [11].

Secondly, due to the weak anharmonicity of the transmon we are exploring a different Hamiltonian than the one implemented with flux qubits. The higher excitation levels of the transmon become increasingly relevant with higher coupling rates and in the USC regime it cannot be considered a two-level system. The system studied here is therefore not a strict implementation of the Rabi model, yet is still expected to bear many of the typical USC features and a proposal has been made to measure them [26].

II. SETUP

Our device, depicted in Fig. 1, consists of a high-impedance superconducting $\lambda/2$ microwave resonator [27] capacitively overcoupled to a 50 Ω feedline on one end and coupled to a transmon qubit on the other. The resonator is a 1 μm wide, 180 nm thick, and ∼6.5 mm long meandering conductor. It is capacitively connected to a background plane through the 275 μm silicon substrate as well as through vacuum/silicon to the side ground planes.

The transmon is in part coupled to ground through a vacuum gap capacitor; see Fig. 1(b). Its bottom electrode constitutes one island of the transmon; the other plate is a suspended 50 nm thick graphite flake. The diameter of this capacitor is 15 μm with a gap of 150 nm. This device was designed to couple the mechanical motion of the suspended graphite to the transmon qubit, where the coupling is mediated by a dc voltage offset [28,29]. In this experiment, the graphite flake is

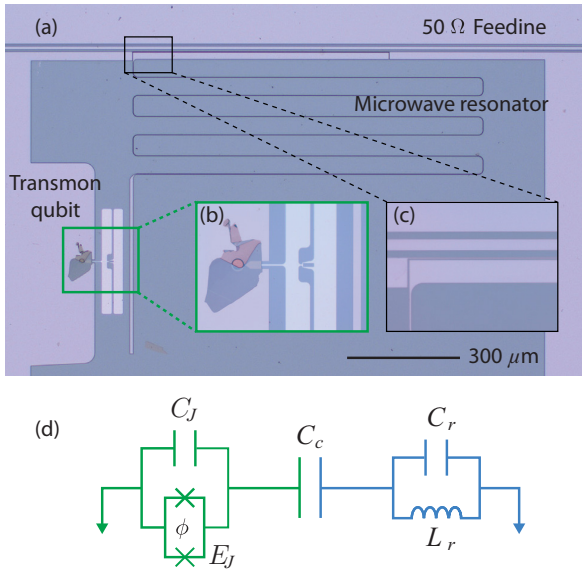

FIG. 1. (a) Optical image of the device, showing the $\lambda/2$-microwave resonator formed by a meandering 1 μm wide stripline capacitively coupled to a 50 Ω feedline on one end and a transmon qubit on the other end. (b) Zoom in on the transmon qubit, showing the SQUID loop formed by two Josephson junctions and the parallel plate vacuum-gap capacitor formed by an aluminum qubit as bottom electrode and graphite as top electrode. (c) Zoom in on the capacitive coupler between the resonator and the feedline. (d) Equivalent lumped element circuit of the device, as derived in the Supplemental Material [21].

however very thick and is not biased by a dc voltage, rendering the coupling of the qubit to the motion negligible. To enable tunability of the qubit frequency, a superconducting quantum interference device (SQUID) loop is incorporated such that the Josephson energy E_J can be modified using an external magnetic field. $E_J(\phi)$ is a function of the flux through the SQUID loop ϕ following $E_J(\phi) = E_{J,\max}\cos(\pi\phi/\phi_0)$, where $\phi_0 = h/2e$ is the superconducting flux quantum.

We fabricate our devices in a three-step process. First we define our microwave resonators on a 275 μm silicon substrate using reactive ion etching of molybdenum-rhenium (MoRe) alloy [30]. Subsequently, Al/AlO_x/Al Josephson junctions are fabricated using aluminum shadow evaporation [31]. Finally, we stamp a graphite flake on the 15 μm diameter opening in the ground plane using a deterministic dry viscoelastic stamping technique [32]. From room temperature resistance measurements, optical, and SEM images we observe that the flake is suspended, though folded, and that it does not short the qubit to ground.

This device implements the circuit shown in Fig. 1 [21]. Following circuit quantization [33], we find that the dynamics of the system are governed by the Hamiltonian

$$\hat{H} = \hbar\omega_r\hat{a}^\dagger\hat{a} + \hbar\omega_a\hat{b}^\dagger\hat{b} - \frac{E_c}{2}\hat{b}^\dagger\hat{b}^\dagger\hat{b}\hat{b} + \hbar g(\hat{a}+\hat{a}^\dagger)(\hat{b}+\hat{b}^\dagger), \tag{2}$$

where $\hat{a}$ ($\hat{b}$) is the annihilation operator for resonator (transmon) excitations. The bare resonator and transmon frequencies are given by $\omega_r = 1/\sqrt{L_r C_{r,\text{eff}}}$, $\omega_a = \sqrt{8E_J E_c} - E_c$, the charging energy is given by $E_c = e^2/2C_{J,\text{eff}}$, and the coupling strength

$$g \simeq \sqrt{\frac{\omega_a\omega_r}{4\left(1+\frac{C_J}{C_c}\right)\left(1+\frac{C_r}{C_c}\right)}}. \tag{3}$$

The dependence on the flux ϕ is omitted in the expression of the coupling strength and transmon frequency for clarity. It is important to distinguish the capacitances C_c, C_J, C_r from the effective capacitances

$$C_{J,\text{eff}} = \frac{C_J C_r + C_J C_c + C_c C_r}{C_r + C_c},$$
$$C_{r,\text{eff}} = \frac{C_J C_r + C_J C_c + C_c C_r}{C_J + C_c}. \tag{4}$$

The former correspond to the physical circuit elements, whereas the latter lead to the correct eigenfrequencies of the resonator and transmon, defined as the oscillation rate of charges through the inductance L_r and Josephson junction, respectively. Using finite-element simulation software, the qubit is designed such that its capacitance to ground $C_J = 51$ fF and its coupling capacitor is $C_c = 9$ fF. The parameters of other circuit elements will be extracted from the data. We will denote the lowest three eigenstates of the transmon by $|g\rangle$, $|e\rangle$, and $|f\rangle$ with increasing energies.

We characterize our device at a temperature of 15 mK, mounted in a radiation-tight box. From a vector network analyzer we send a microwave tone that is heavily attenuated before being launched on the feedline of the chip. The transmitted signal is send back to the vector network analyzer through a circulator and a low-noise high-electron-mobility transistor amplifier. This setup is detailed in the Supplemental Material [21]. It allows us to probe the absorption of our device and thus the energy spectrum of the Hamiltonian (2). At high driving power we measure the bare cavity resonance [34] to have a total linewidth of $\kappa = 2\pi \times 29.3$ MHz and a coupling coefficient of $\eta = \kappa_c/\kappa = 0.96$, giving the ratio between the coupling rate κ_c and total dissipation rate $\kappa = \kappa_c + \kappa_i$, where κ_i is the internal dissipation rate.

III. RESULTS

With a current biased coil, we can control the magnetic field and tune the effective E_J to bring the qubit in resonance with the cavity. Where the transmon and resonator frequencies cross, we measure a vacuum Rabi splitting which gives an estimate of the coupling rate $2g/2\pi \simeq 910$ MHz as shown in Fig. 2.

In Fig. 3, we show the result of performing two-tone spectroscopy to probe the qubit frequency [35,36]. When the qubit is detuned from the cavity, the resonator acquires a frequency shift which is dependent on the state of the qubit. Hence probing the transmission of the feedline at the cavity resonance (shifted by the qubit in the ground state), while exciting the qubit with another microwave tone, will cause the transmission to change by a value $\delta|S_{21}|$ due to the qubit-state dependent shift. In Fig. 3(a) we measure the spectral response of the qubit for different magnetic fields. As the magnetic flux through the SQUID loop tunes the qubit frequency we track the ground to first excited state transition as a function of magnetic field. Since the probe power is kept constant during this experiment a clear power broadening of

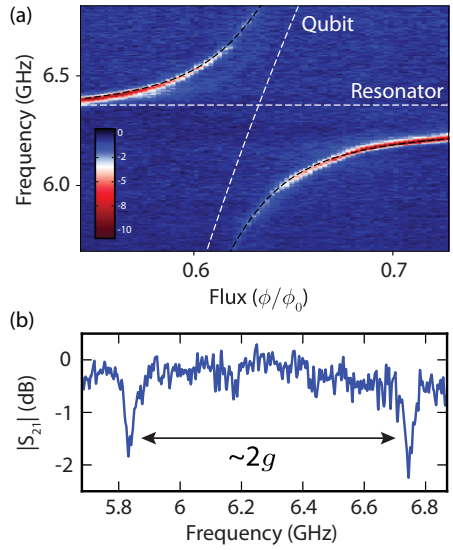

FIG. 2. (a) Color plot of the feedline transmission $|S_{21}|$ as a function of magnetic field and frequency, showing the coupling between the resonator and qubit. The magnetic flux penetrating the SQUID loop incorporated in the transmon qubit changes the Josephson energy, which results in the tunability of the $|g\rangle - |e\rangle$ transition energy of the qubit. Close to resonance the qubit and resonator show an avoided crossing centered at 6.23 GHz. Black dashed lines correspond to fits to this data. The horizontal (oblique) white dashed line corresponds to the bare resonator (transmon) frequency, $\omega_r/2\pi$ [$\omega_a(\phi)/2\pi$]. The lack of symmetry around the crossing point is due to the flux dependence of the coupling strength g. (b) Trace of the microwave response where the qubit and cavity are close to resonance $\phi = 0.63\phi_0$ showing an anticrossing of $2g \simeq 2\pi \times 910$ MHz and a linewidth of 28 MHz.

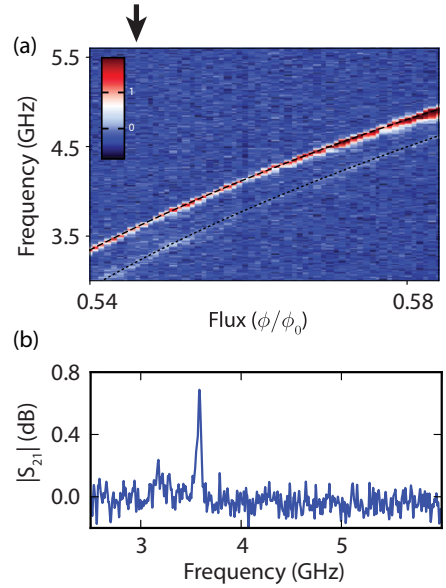

FIG. 3. (a) Color plot of the change in transmission ($\delta|S_{21}|$) of a microwave tone at resonance with the cavity at single-photon power as a function of frequency of a secondary qubit-drive tone and magnetic field. Due to the qubit-state dependent frequency shift of the cavity, the transmission changes as the drive tone excites the qubit, tracing the qubit $|g\rangle - |e\rangle$ transition frequency as a function of magnetic field. The secondary faint resonance corresponds to the $|e\rangle - |f\rangle$ transition of the thermally excited population in state $|e\rangle$. Power broadening is visible when the qubit transition frequency is close to the cavity. The power of the drive tone delivered to the feedline is constant, but close to the cavity a larger portion of the power is delivered to the qubit. Dashed lines correspond to fits to the data. (b) Line cut of the color plot where the qubit frequency is at $\omega_a = 2\pi \times 3.586$ GHz with a linewidth of 38 MHz. The second peak corresponds to the first to second exited state transition, which corresponds to the (dressed) anharmonicity, a rough approximation of $E_c/h = 370$ MHz.

the qubit is visible, because more of the power is delivered to the qubit as it is closer to the cavity in frequency. The secondary faint resonance corresponds to the spectral response of the first to second exited state transition of the transmon due to some residual occupation of the first excited state. The difference in frequency between both transitions provides an estimate of the charging energy (or equivalently the anharmonicity of the transmon), $E_c/h \sim 370$ MHz. In reality what we measure is a quantity that is dressed by the interaction with the cavity and diverges from the bare value of E_C.

The 38 MHz linewidth of this resonance translates to very short coherence times ($T_1 \sim 40$ ns) compared to typical implementations [37]. Purcell losses contribute less than 2 MHz to this linewidth. The ohmic losses in the graphite can also not explain this high dissipation. From the bulk conductivity of graphite, we find that the resistance of our 50 nm thick flake is 7 $\Omega/\square$ [38]. Simulating the effect of a 7 Ω resistance at the appropriate position in the qubits capacitance network using QUCS [39] reveals that this has a negligible contribution of 200 kHz to the total transmon linewidth. Other possibilities include dielectric losses in the interface between silicon and MoRe. Indeed, the high quality factors previously obtained with this superconductor [30] were very sensitive to a surface preponderation which was incompatible with the complexity of the device presented here. Another relevant source of dissipation could be the resistance associated with the conversion of a supercurrent into a normal current at the interface between MoRe and the graphite [40].

We fit a numerical diagonalization of the Hamiltonian detailed in the Supplemental Material [21] to the acquired data, obtaining the fits shown as dashed lines in Figs. 2 and 3. We thereby obtain the Hamiltonian parameters $E_c/h = 300$ MHz, $g/2\pi = 455$ MHz (on resonance), $\omega_r/2\pi = 6.367$ GHz, and $E_{J,\max}/h = 46$ GHz. Combined with our knowledge of the capacitances C_J and C_c, we extract the following values for the circuit elements of the resonator: $C_r = 57.1$ fF and $L_r = 9.65$ nH. If we assume that the parallel LC oscillator corresponds to the fundamental mode of a $\lambda/2$ resonator, then the resonators effective impedance $Z_r = \sqrt{L_r/C_r} = 411\ \Omega$ is related to the characteristic impedance of the transmission line through $Z_0 = \pi Z_r/2$ [21], yielding a value $Z_0 = 645\ \Omega$.

IV. TOWARDS HIGHER COUPLING IN TRANSMON SYSTEMS: A PROPOSAL

In the circuit of Fig. 1(d), the coupling rate is limited following

$$\frac{g}{\sqrt{\omega_a \omega_r}} = \frac{1}{2}\sqrt{\frac{1}{1+\frac{C_J}{C_c}}\frac{1}{1+\frac{C_r}{C_c}}} \leqslant \frac{1}{2}. \tag{5}$$

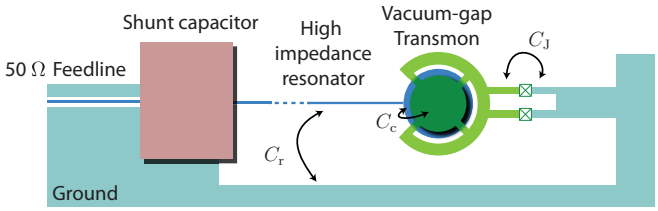

FIG. 4. Proposal for larger couplings which combines the use of a $\lambda/4$ high-impedance resonator and a vacuum gap transmon. The $\lambda/4$ can be coupled to a 50 Ω feedline through the use of a shunt capacitor [44]. For $C_J = C_r = 10$ fF and $C_c = 200$ fF the system is expected to reach far into the USC regime $\bar{g} = 0.45$ on resonance.

The highest couplings are therefore achieved by maximizing two capacitance ratios: C_c/C_J and C_c/C_r. In the language of cavity QED with natural atoms, maximizing the first ratio is equivalent to increasing the dipole moment of the atom which is done by using Rydberg atoms [1]. Maximizing the second ratio increases the vacuum fluctuations of the cavities electric field as performed in alkali-atom experiments in a very small optical cavity [41].

In the regime $C_c/C_J, C_c/C_r \gg 1$ the effective capacitances of Eq. (4) are approximated by

$$C_{J,\text{eff}} = C_{r,\text{eff}} \simeq C_J + C_r, \tag{6}$$

these capacitances being the quantities to minimize to increase the coupling. Maximizing the coupling while keeping the resonator and transmon frequencies constant therefore requires a large increase in the inductances. In other words, the higher the impedance of the resonator and the higher the ratio E_c/E_J in the transmon, the higher the coupling.

The highest ratio of E_c/E_J for which we remain in the transmon regime is $\sim 1/20$ [18]. Combined with a typical choice of the transmon frequency $\omega_a/2\pi = 6$ GHz, compatible with most microwave experimental setups, we obtain a value of the transmons total capacitance $C_{J,\text{eff}} = C_{r,\text{eff}} \simeq C_J + C_r \simeq 20$ fF. Choosing $C_J = C_r = 10$ fF maximizes Eq. (5). Fixing the resonator frequency to $\omega_r = \omega_a$ leads to a value for resonators characteristic impedance: 722 Ω if a $\lambda/4$ resonator is used, 1.44 kΩ for a $\lambda/2$ resonator, and 918 Ω for a lumped element resonator. The coupling achieved now depends on the value of the coupling capacitor. For $C_c = 200$ fF, for example, $\bar{g} = 0.45$ and the system is deep in the USC regime.

In Ref. [20], the USC regime was reached by increasing the first capacitance ratio of Eq. (5), $C_c/(C_J + C_c) \simeq 0.9$, through the use of a vacuum-gap coupling capacitor. In this work, the large coupling is reached by increasing the second ratio $C_c/(C_r + C_c) \simeq 0.136$ above the usual values through the use of a high-impedance resonator while the first capacitance ratio remains modest $C_J/(C_J + C_c) \simeq 0.15$. Combining both approaches into a single device represented schematically in Fig. 4 would allow experimentally reaching deep into the USC regime $\bar{g} = 0.45$ by matching the circuit parameters presented previously. The values $C_J = 10$ fF and $C_c = 200$ fF can be easily achieved experimentally reproducing the vacuum-gap transmon architecture of Ref. [20] with a smaller gap and larger capacitive plate, maybe even by replacing the vacuum gap by a dielectric. The use of a $\lambda/4$ resonator rather than a $\lambda/2$ is preferable as it decreases the impedance needed as well as increases the frequency spacing between the fundamental and higher modes. Moving to a $\lambda/4$ resonator makes the current architecture sufficient in terms of resonator impedance. The impedance could be further increased using a high kinetic inductance based resonator [42] or by using an array of Josephson junctions [43].

This proposal is however limited by the underlying assumption that only a single mode of the resonator participates in the dynamics of the system. However, for larger coupling rates, the higher modes no longer play a weak perturbative role [45]. Exploring the exact consequences of this fact on the observable USC phenomena that can be observed is outside the scope of this work, as is determining alternatives to probing the system spectroscopically to show for example the nontrivial ground state that one would expect in this regime. For a detailed study of these topics, we refer the reader to Ref. [26].

V. CONCLUSION

We have shown that it is possible to enhance the coupling between a microwave resonator and a transmon qubit by increasing the impedance of the resonator to 645 Ω compared to typical 50 Ω implementations. In doing this we reach a coupling rate of $g/2\pi = 455$ MHz at resonance, which is close to the ultrastrong coupling regime ($\bar{g} = 0.071$). We have shown that by optimizing this strategy through sources of high inductance, combined with a vacuum-gap transmon architecture, we have the potential of reaching far into the ultrastrong coupling regime.

ACKNOWLEDGMENTS

The authors thank Alessandro Bruno, Leo DiCarlo, Nathan Langford, Adrian Parra-Rodriguez, and Marios Kounalakis for useful discussions. This project has received funding from the Dutch Foundation for Fundamental Research on Matter (FOM), the European Research Council (ERC) under the European Union's Horizon 2020 research and innovation program (Grant Agreement No. 681476–QOMD), and from the Netherlands Organisation for Scientific Research (NWO) in the Innovational Research Incentives Scheme–VIDI, Project No. 680-47-526.

S.J.B. and M.F.G. contributed equally to this manuscript.

[1] J. M. Raimond, M. Brune, and S. Haroche, Rev. Mod. Phys. **73**, 565 (2001).

[2] A. Wallraff, D. I. Schuster, A. Blais, L. Frunzio, R.-S. Huang, J. Majer, S. Kumar, S. M. Girvin, and R. J. Schoelkopf, Nature (London) **431**, 162 (2004).

[3] E. T. Jaynes and F. W. Cummings, Proc. IEEE **51**, 89 (1963).

[4] I. I. Rabi, Phys. Rev. **49**, 324 (1936).

[5] D. Braak, Q.-H. Chen, M. T. Batchelor, and E. Solano, J. Phys. A: Math. Theor. **49**, 300301 (2016).

[6] D. Z. Rossatto, C. J. Villas-Bôas, M. Sanz, and E. Solano, arXiv:1612.03090.

[7] Q. Xie, H. Zhong, M. T. Batchelor, and C. Lee, J. Phys. A: Math. Theor. **50**, 113001 (2017).

[8] J. Casanova, G. Romero, I. Lizuain, J. J. García-Ripoll, and E. Solano, Phys. Rev. Lett. **105**, 263603 (2010).

[9] L. Garziano, R. Stassi, A. Ridolfo, O. Di Stefano, and S. Savasta, Phys. Rev. A **90**, 043817 (2014).

[10] G. Romero, D. Ballester, Y. M. Wang, V. Scarani, and E. Solano, Phys. Rev. Lett. **108**, 120501 (2012).

[11] R. Stassi and F. Nori, arXiv:1703.08951.

[12] T. Niemczyk, F. Deppe, H. Huebl, E. P. Menzel, F. Hocke, M. J. Schwarz, J. J. Garcia-Ripoll, D. Zueco, T. Hümmer, E. Solano, A. Marx, and R. Gross, Nat. Phys. **6**, 772 (2010).

[13] P. Forn-Díaz, J. Lisenfeld, D. Marcos, J. J. García-Ripoll, E. Solano, C. J. P. M. Harmans, and J. E. Mooij, Phys. Rev. Lett. **105**, 237001 (2010).

[14] F. Yoshihara, T. Fuse, S. Ashhab, K. Kakuyanagi, S. Saito, and K. Semba, Nat. Phys. **13**, 44 (2017).

[15] P. Forn-Díaz, J. J. García-Ripoll, B. Peropadre, J.-L. Orgiazzi, M. A. Yurtalan, R. Belyansky, C. M. Wilson, and A. Lupascu, Nat. Phys. **13**, 39 (2016).

[16] N. K. Langford, R. Sagastizabal, M. Kounalakis, C. Dickel, A. Bruno, F. Luthi, D. J. Thoen, A. Endo, and L. DiCarlo, arXiv:1610.10065.

[17] J. Braumüller, M. Marthaler, A. Schneider, A. Stehli, H. Rotzinger, M. Weides, and A. V. Ustinov, arXiv:1611.08404.

[18] J. Koch, T. M. Yu, J. Gambetta, A. A. Houck, D. I. Schuster, J. Majer, A. Blais, M. H. Devoret, S. M. Girvin, and R. J. Schoelkopf, Phys. Rev. A **76**, 042319 (2007).

[19] A. Stockklauser, P. Scarlino, J. V. Koski, S. Gasparinetti, C. K. Andersen, C. Reichl, W. Wegscheider, T. Ihn, K. Ensslin, and A. Wallraff, Phys. Rev. X **7**, 011030 (2017).

[20] S. J. Bosman, M. F. Gely, V. Singh, A. Bruno, D. Bothner, and G. A. Steele, arXiv:1704.06208.

[21] See Supplemental Material at http://link.aps.org/supplemental/10.1103/PhysRevB.95.224515 for a derivation of the circuit Hamiltonian and further details on the experimental setup, which includes Refs. [46–48].

[22] Also derived in T. Jaako, Z.-L. Xiang, J. J. Garcia-Ripoll, and P. Rabl, Phys. Rev. A **94**, 033850 (2016), although differing by a factor of 2 due to a different definition of g.

[23] M. Takita, A. D. Córcoles, E. Magesan, B. Abdo, M. Brink, A. Cross, J. M. Chow, and J. M. Gambetta, Phys. Rev. Lett. **117**, 210505 (2016).

[24] J. Kelly, R. Barends, A. G. Fowler, A. Megrant, E. Jeffrey, T. C. White, D. Sank, J. Y. Mutus, B. Campbell, Y. Chen, Z. Chen, B. Chiaro, A. Dunsworth, I.-C. Hoi, C. Neill, P. J. J. O'Malley, C. Quintana, P. Roushan, A. Vainsencher, J. Wenner, A. N. Cleland, and J. M. Martinis, Nature (London) **519**, 66 (2015).

[25] D. Ristè, S. Poletto, M.-Z. Huang, A. Bruno, V. Vesterinen, O.-P. Saira, and L. DiCarlo, Nat. Commun. **6**, 6983 (2015).

[26] C. K. Andersen and A. Blais, New J. Phys. **19**, 023022 (2017).

[27] D. M. Pozar, *Microwave Engineering* (John Wiley & Sons, New York, 2009).

[28] M. D. LaHaye, J. Suh, P. M. Echternach, K. C. Schwab, and M. L. Roukes, Nature (London) **459**, 960 (2009).

[29] J.-M. Pirkkalainen, S. U. Cho, F. Massel, J. Tuorila, T. T. Heikkilä, P. J. Hakonen, and M. A. Sillanpää, Nat. Commun. **6**, 6981 (2015).

[30] V. Singh, B. H. Schneider, S. J. Bosman, E. P. J. Merkx, and G. A. Steele, Appl. Phys. Lett. **105**, 222601 (2014).

[31] G. J. Dolan, Appl. Phys. Lett. **31**, 337 (1977).

[32] A. Castellanos-Gomez, M. Buscema, R. Molenaar, V. Singh, L. Janssen, H. S. J. van der Zant, and G. A. Steele, 2D Mater. **1**, 011002 (2014).

[33] M. H. Devoret, *Quantum Fluctuations in Electrical Circuits: Les Houches Session LXIII* (Elsevier Science B. V., Amsterdam, The Netherlands, 1997), p. 351.

[34] L. S. Bishop, E. Ginossar, and S. M. Girvin, Phys. Rev. Lett. **105**, 100505 (2010).

[35] A. Blais, R.-S. Huang, A. Wallraff, S. M. Girvin, and R. J. Schoelkopf, Phys. Rev. A **69**, 062320 (2004).

[36] A. Wallraff, D. I. Schuster, A. Blais, L. Frunzio, J. Majer, M. H. Devoret, S. M. Girvin, and R. J. Schoelkopf, Phys. Rev. Lett. **95**, 060501 (2005).

[37] A. A. Houck, J. A. Schreier, B. R. Johnson, J. M. Chow, J. Koch, J. M. Gambetta, D. I. Schuster, L. Frunzio, M. H. Devoret, S. M. Girvin, and R. J. Schoelkopf, Phys. Rev. Lett. **101**, 080502 (2008).

[38] W. Primak and L. H. Fuchs, Phys. Rev. **95**, 22 (1954).

[39] M. E. Brinson and S. Jahn, Int. J. Numer. Model. **22**, 297 (2009).

[40] G. R. Boogaard, A. H. Verbruggen, W. Belzig, and T. M. Klapwijk, Phys. Rev. B **69**, 220503 (2004).

[41] R. J. Thompson, G. Rempe, and H. J. Kimble, Phys. Rev. Lett. **68**, 1132 (1992).

[42] N. Samkharadze, A. Bruno, P. Scarlino, G. Zheng, D. P. DiVincenzo, L. DiCarlo, and L. M. K. Vandersypen, Phys. Rev. Appl. **5**, 044004 (2016).

[43] N. A. Masluk, I. M. Pop, A. Kamal, Z. K. Minev, and M. H. Devoret, Phys. Rev. Lett. **109**, 137002 (2012).

[44] S. J. Bosman, V. Singh, A. Bruno, and G. A. Steele, Appl. Phys. Lett. **107**, 192602 (2015).

[45] M. F. Gely, A. Parra-Rodriguez, D. Bothner, Y. M. Blanter, S. J. Bosman, E. Solano, and G. A. Steele, Phys. Rev. B **95**, 245115 (2017).

[46] R. M. Foster, Bell Syst. Tech. J. **3**, 259 (1924).

[47] S. E. Nigg, H. Paik, B. Vlastakis, G. Kirchmair, S. Shankar, L. Frunzio, M. H. Devoret, R. J. Schoelkopf, and S. M. Girvin, Phys. Rev. Lett. **108**, 240502 (2012).

[48] B. C. Wadell, *Transmission Line Design Handbook* (Artech House, Boston, 1991).